Non-Heme Iron Complexes

Deutsche Ausgabe: DOI: 10.1002/ange.201911968
Internationale Ausgabe: DOI: 10.1002/anie.201911968

The $Fe_2(NO)_2$ Diamond Core: A Unique Structural Motif In Non-Heme Iron–NO Chemistry

*Hai T. Dong, Amy L. Speelman, Claire E. Kozemchak, Debangsu Sil, Carsten Krebs, and Nicolai Lehnert**

Dedicated to Professor Felix Tuczek on the occasion of his 60th birthday.

Abstract: *Non-heme high-spin (hs) {FeNO}^{8} complexes have been proposed as important intermediates towards N_2O formation in flavodiiron NO reductases (FNORs). Many hs-{FeNO}^{8} complexes disproportionate by forming dinitrosyl iron complexes (DNICs), but the mechanism of this reaction is not understood. While investigating this process, we isolated a new type of non-heme iron nitrosyl complex that is stabilized by an unexpected spin-state change. Upon reduction of the hs-{FeNO}^{7} complex, [Fe(TPA)(NO)(OTf)](OTf) (**1**), the N-O stretching band vanishes, but no sign of DNIC or N_2O formation is observed. Instead, the dimer, $[Fe_2(TPA)_2(NO)_2](OTf)_2$ (**2**) could be isolated and structurally characterized. We propose that **2** is formed from dimerization of the hs-{FeNO}^{8} intermediate, followed by a spin state change of the iron centers to low-spin (ls), and speculate that **2** models intermediates in hs-{FeNO}^{8} complexes that precede the disproportionation reaction.*

Nitric oxide (NO) is ubiquitous in biological systems and serves, for example, as a signaling molecule that regulates blood pressure and mediates nerve signal transduction in mammals at low, nanomolar concentrations.[1] Higher concentrations of NO are acutely toxic and are used by mammals for immune defense.[2] More recently, the one-electron-reduced form of NO, nitroxyl (NO^-/HNO), has been shown to mediate a wide range of biological responses.[3] For example, both ferric and ferrous hemes are capable of binding HNO to form {FeNO}^{7} and {Fe(H)NO}^{8} complexes, respectively.[4] Such {Fe(H)NO}^{8} type species have also been proposed as key intermediates in the catalytic cycles of fungal NO reductase cytochrome (Cyt; P450nor) and multiheme Cyt *c* nitrite reductase.[5] In contrast, the coordination chemistry of non-heme iron centers with nitroxyl is not well developed. Recent studies on model complexes for flavodiiron NO reductases (FNORs) have demonstrated that stable high-spin (hs) diferrous dinitrosyl complexes, [hs-{FeNO}^{7}]$_2$, can be activated by reduction to the hs-{FeNO}^{8}, or Fe^{II}-nitroxyl, state for N_2O formation.[6] FNORs are important enzymes in bacterial pathogenesis, as they protect infectious microbes from the mammalian immune defense agent NO.[7] Whereas few mononuclear non-heme iron-NO model complexes have been shown to generate N_2O upon reduction to the hs-{FeNO}^{8} state,[8] a major reactivity of these complexes seems to be disproportionation, leading to the formation of dinitrosyl iron complexes (DNICs) [Eq. (1)]:[9]

$$2\,\text{hs-}\{\text{FeNO}\}^7 + 2\,e^- \rightarrow 2\,\text{hs-}\{\text{FeNO}\}^8 \rightarrow \{\text{Fe(NO)}_2\}^{10} + \text{Fe}^{II} \quad (1)$$

However, the mechanism of this disproportionation, which constitutes an elegant pathway for the generation of DNICs from simple non-heme iron centers, is unknown. Clearly, more work is necessary to elucidate the biologically-relevant reactivity of non-heme hs-{FeNO}^{8} complexes. DNICs of {Fe(NO)$_2$}$^{9/10}$ type are important in mammalian physiology, as they serve as a major pool of NO.[10] In addition, DNICs with histidine ligation have been proposed to form at the non-heme diiron core of the ferric uptake regulation protein (Fur),[11] in serum albumin,[12] and in ferritin.[13] In this regard, understanding the reactivity of hs-{FeNO}^{8} complexes provides important insight into how diiron sites can be predispositioned for the diverging functions of N_2O or DNIC formation. However, the unstable nature of non-heme hs-{FeNO}^{8} complexes has so far prevented the isolation of any intermediates prior to DNIC formation.[14]

Herein, we further investigated the reactivity of hs-{FeNO}^{8} complexes with TPA (tris(2-pyridylmethyl)amine) and related coligands. In particular, we report the serendipitous discovery of a $Fe_2(NO)_2$ diamond core structure, which is unprecedented in non-heme iron-NO chemistry. This core structure is stabilized by a change in spin state of the iron centers to low-spin (ls) Fe^{II}. In contrast, a TPA derivative with a weaker ligand field that cannot support the spin-state change to ls proceeds to DNIC formation. These complexes were further characterized by X-ray crystallography, and Mössbauer and vibrational spectroscopy.

The ligand TPA was synthesized according to reported procedures, and characterized by ^{1}H NMR spectroscopy.[15] Metallation of TPA was carried out using $Fe(OTf)_2{\cdot}2\,CH_3CN$

[*] H. T. Dong, Dr. A. L. Speelman, C. E. Kozemchak, Prof. N. Lehnert
Department of Chemistry and Department of Biophysics
The University of Michigan
Ann Arbor, Michigan 48109-1055 (USA)
E-mail: lehnertn@umich.edu
Dr. D. Sil, Prof. C. Krebs
Department of Chemistry and Department of Biochemistry and Molecular Biology
The Pennsylvania State University
University Park, Pennsylvania 16802 (USA)
Supporting information and the ORCID identification number(s) for the author(s) of this article can be found under: https://doi.org/10.1002/anie.201911968.

in CH_3CN to obtain a pure red solid of $[Fe(TPA)(CH_3CN)_2](OTf)_2$. Synthesis of $[Fe(TPA)(NO)(OTf)](OTf)$ (**1**) was accomplished by treating the red solution of $[Fe(TPA)(CH_3CN)_2](OTf)_2$ in CH_3CN with excess NO gas, which led to an immediate color change to black. Complex **1** was isolated as a pure black solid upon crystallization. The formation of **1** is evident from UV/Vis spectroscopy, which shows the disappearance of the intense bands at 320 and 380 nm of the ferrous precursor, and the appearance of new bands at 326, 403, 490, and 655 nm upon reaction with NO (Figure S1 in the Supporting Information). The solid state IR spectrum of complex **1** shows the characteristic N–O stretching band of a hs-$\{FeNO\}^7$ complex at 1806 cm^{-1}, which shifts to 1766 cm^{-1} with ^{15}NO and 1732 cm^{-1} with $^{15}N^{18}O$ (Figure S3). The cyclic voltammogram of **1** is unusual, and shows two irreversible redox events at −690 mV and −1240 mV versus Fc^+/Fc ($Fc = [(\eta\text{-}C_5H_5)_2Fe]$), respectively (Figure S11). The first event corresponds to the one-electron reduction of complex **1**, forming an unstable hs-$\{FeNO\}^8$ complex, **1red**. This wave remains irreversible, even when the scan is stopped prior to the second redox event. The second redox event likely originates from a new species formed from **1red**. EPR spectra of **1** in CH_2Cl_2 show an axial signal at $g_{eff} = 3.91$ and 2.00, characteristic of a hs-$\{FeNO\}^7$ complex with $S_t = 3/2$ (Figure S13, top). Surprisingly, the EPR spectrum of **1** in CH_3CN shows a new EPR signal at $g = 2$, indicating the partial formation of a ls-$\{FeNO\}^7$ complex with $S_t = 1/2$ in this solvent (Figure S13, top). This observation is supported by the appearance of a new signal at 1701 cm^{-1} in the solution IR spectrum of **1** in CH_3CN (Figure S13, bottom). In this regard it should be noted that ferrous TPA complexes are close to the spin crossover point as previously reported.[16] In our case, the coordination of the solvent CH_3CN is likely responsible for the spin change behavior, according to the equilibrium [Eq. (2)]:

$$[Fe(TPA)(NO)(OTf)]^+ + CH_3CN \rightleftharpoons [Fe(TPA)(NO)(CH_3CN)]^{2+} + OTf^- \quad (2)$$

where the CH_3CN-coordinated compound is then ls. To test this hypothesis further, we prepared the analogous hs-$\{FeNO\}^7$ complex with the weakly-coordinating tetrafluoroborate (BF_4^-) counter ion, **1-BF_4**. In the solid state, this complex shows the N-O stretch at 1795 cm^{-1}. In CH_3CN solution, the EPR spectrum of **1-BF_4** now shows the major signal at $g = 2.00$, indicating dominant formation of the ls ($S_t = 1/2$) complex $[Fe(TPA)(NO)(CH_3CN)])(BF_4)_2$ (Figure S18). In the solution IR spectrum of **1-BF_4** in CH_3CN, the N-O stretch of the ls component is observed at 1701 cm^{-1}, identical to complex **1** in CH_3CN, indicating that the same ls species forms. These observations strongly support our hypothesis that CH_3CN-coordination is the cause for the spin state change in complex **1**. This conclusion is further support by density functional theory (DFT) calculations (B3LYP*/TZVP), which show that the hs state of complex **1** is 3 kcal mol^{-1} lower in energy in comparison to the ls state. Upon replacing the bound triflate in **1** with a CH_3CN solvent molecule, the hs and ls states become isoenergetic, with the ls state at slightly lower energy (0.34 kcal mol^{-1}). Spin density analysis shows that the ls complex (with CH_3CN bound) has a Fe^{II}-$NO^{\bullet}$ type electronic structure, typically observed for six-coordinate ferrous heme-nitrosyls.[17]

Crystals suitable for X-ray diffraction were obtained via diffusion of diethyl ether into a saturated solution of **1** in acetonitrile (Figure 1). As has been observed previously for

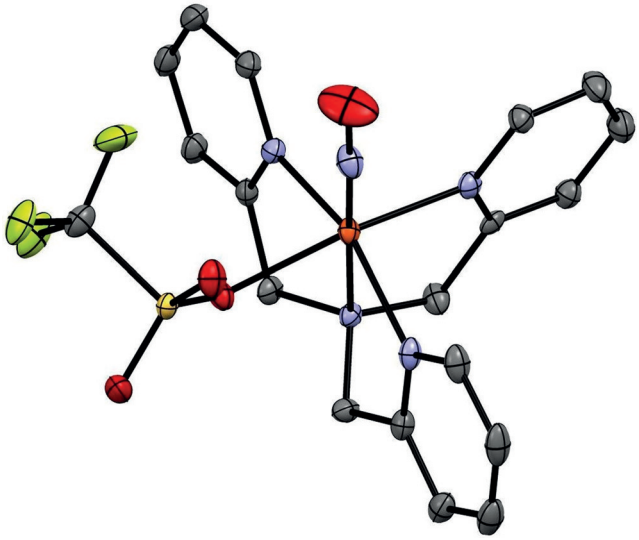

Figure 1. Crystal structure of complex **1** with thermal ellipsoids set at 50% probability. The triflate counter anion, solvent molecules, and hydrogen atoms are omitted for clarity. Fe orange, O red, N light blue, C gray, S pale yellow, F yellow.[21]

other non-heme hs-$\{FeNO\}^7$ complexes, **1** exhibits a pseudo-octahedral geometry with a triflate counter ion bound in the sixth coordination site. Complex **1** shows Fe–NO and N–O bond lengths of 1.76 and 1.14 Å, respectively. Interestingly, the Fe-N-O angle is 170°, which is surprising, considering that there is not much steric hindrance present in the TPA ligand scaffold. Similar linear Fe-N-O angles have been observed in other hs-$\{FeNO\}^7$ complexes with ν(N-O) > 1800 cm^{-1}.[18] This indicates that the linear Fe-N-O angle in **1** originates from electronic factors, that is, a very covalent Fe-NO bond due to an electron-poor Fe center.[18,19]

Upon reduction of **1** with 1 equivalent of $CoCp_2$ in CH_2Cl_2 (in which **1** is 100% hs; $Cp = \eta\text{-}C_5H_5$) the solution immediately changes color from black to bright orange, indicating the formation of a new species (**2**). The UV/Vis spectroscopic titration of **1** with $CoCp_2$ shows a complete transformation of **1** with one equivalent of reductant via appearance of a new, highly intense band at 445 nm (Figure S2). Both solid state and solution IR spectra show the disappearance of the intense N–O stretching band of **1** upon reduction to **2** (Figure 3 and Figure S6), but surprisingly, no new band is observed at approximately 2220 cm^{-1} (expected for N_2O) and within the 1600–1800 cm^{-1} region (expected for DNIC and hs-$\{FeNO\}^8$ complexes). This indicates the possibility of NO dissociation from our metal complex upon reduction. However, mass spectrometry shows m/z 376.09 that shifts to 377.09 with ^{15}NO and 379.09 with $^{15}N^{18}O$ (Figure S19,20). This proves that NO is still bound to the reduction product; however, the N–O

stretch must have somehow shifted to significantly lower energy ($<1500\,cm^{-1}$). At the same time, the ^1H NMR spectrum of the isolated product **2** shows a normal NMR spectrum, and all the protons of the ligand scaffold can be identified and integrated accordingly (Figure S22). The Evans method further confirms that the compound is strictly diamagnetic at room temperature. The Mössbauer isomer shift of **2** ($\delta = 0.31\,mm\,s^{-1}$) supports the formation of diamagnetic low-spin Fe^{II} centers (see Figure 4). This suggests the clean formation of an $S_t = 0$ species upon reduction of **1**, instead of the expected DNIC formation according to Equation (1).

To determine the exact nature of the reduced product, crystals suitable for X-ray diffraction were grown from diffusion of diethyl ether into a saturated solution of **2** in acetonitrile. To our surprise, complex **2** is formed by the dimerization of two hs-{FeNO}^{8} units, bridged by the two NO molecules (Figure 2), with a molecular formula of $[Fe_2(TPA)_2(NO)_2](OTf)_2$. To our knowledge, this is the first

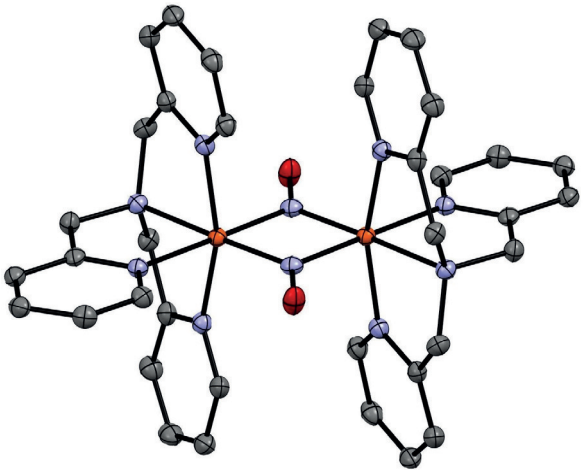

Figure 2. Crystal structure of complex **2** with thermal ellipsoids set at 50% probability. The triflate counter anion, solvent molecules, and hydrogen atoms are omitted for clarity.[21]

observation of an $Fe_2(NO)_2$ diamond core in non-heme iron-NO chemistry. Further characterization by IR spectroscopy reveals the antisymmetric (as) N–O stretching frequency of **2** at 1350 cm^{-1} that shifts to 1330 cm^{-1} with ^{15}NO and 1306 cm^{-1} with $^{15}N^{18}O$ (Figure 3 and Figure S4). In comparison, the hs-{FeNO}^{8} complex $[Fe(TMG_3tren)(NO)]^+$ shows ν(N-O) at 1618 cm^{-1}.[14] The low N-O stretching frequencies observed for **2** indicate coordination of singlet NO^-, that is, complex **2** contains two ls-Fe^{II} centers ($S = 0$) bound to two $^1NO^-$ units ($S = 0$) and is therefore strictly diamagnetic.

To further explore the electronic properties of this new complex, DFT calculations were performed. Geometry optimization of **2** with diamagnetic, bridged ls-{FeNO}^{8} centers (using BP86/TZVP, which has been shown to give good structures for nitrosyl complexes)[20] shows good agreement with the structural parameters of **2** (Table S22). Subsequent frequency calculations predict $\upsilon_{as}(N\text{-}O) = 1364\,cm^{-1}$ and $\upsilon_{sym}(N\text{-}O) = 1399\,cm^{-1}$ with BP86/TZVP,

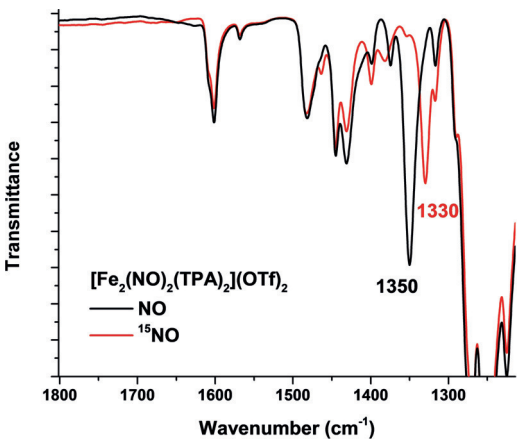

Figure 3. IR spectra of solid samples of complex **2** with natural abundance isotopes (n.a.i.) NO (black) and ^{15}NO (red).

where $\upsilon_{sym}(N\text{-}O)$ is not IR active (due to the centrosymmetric $Fe_2(NO)_2$ diamond core). The calculated $\upsilon_{as}(N\text{-}O)$ is in very good agreement with experiment. Calculated Mössbauer parameters are also in excellent agreement with experimentally determined parameters ($\delta = 0.31(exp)/0.28(calc)\,mm\,s^{-1}$ and $|\Delta E_Q| = 1.40(exp)/1.66(calc)\,mm\,s^{-1}$) and indicate that the Fe centers are in the ls + II state (Figure 4). As predicted by DFT, we do not observe the symmetric N–O stretch of complex **2**. Interestingly, DFT calculations with hybrid functionals like B3LYP overestimate the stretching frequencies of the bridging NO ligands in the diamond core (see Table S25). In addition, calculations where both of the iron centers are in the hs state immediately collapse to the $S_t = 0$ spin state with various functional and basis set combinations, suggesting that the ls state of this complex is favorable, thus preventing us from directly calculating the energy of the analogue of **2** where the Fe^{II} centers are hs.

As a control, we prepared an analogous complex with a ligand that provides a weaker ligand field (according to the

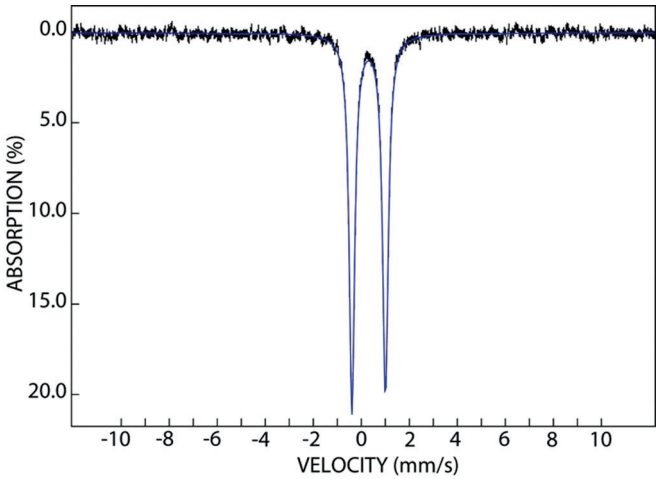

Figure 4. Mössbauer spectrum of complex **2** recorded at 4.2 K in an external 53-mT magnetic field applied parallel to the propagation direction of the γ beam. The experimental data are shown as black vertical bars. The blue line is a simulation using the following parameters: $\delta = 0.31\,mm\,s^{-1}$, $|\Delta E_Q| = 1.40\,mm\,s^{-1}$.

spectrochemical series), to test whether formation of complex **2** is dependent on the ligand field strength. Previous studies have shown fast DNIC formation following reduction of our hs-{FeNO}^{8} model complex, [Fe(TMG$_2$dien)(NO)]$^+$.[14] Similar reactivity is observed for our new hs-{FeNO}^{7} complex [Fe(BMPA-tBu$_2$PhO)(NO)(OTf)] (**3**), which contains the weak field ligand [N-(3,5-di-tert-butyl-2-hydroxybenzyl)-*N*,*N*-di-(2-pyridylmethyl)]amine (BMPA-tBu$_2$PhOH). The metallation of BMPA-tBu$_2$PhOH was carried out using KOMe and Fe(OTf)$_2$·2 CH$_3$CN in MeOH to obtain a pure yellow solid of [Fe(BMPA-tBu$_2$PhO)(OTf)] after purification. Nitrosylation of this yellow solid in THF using dried NO gas resulted in the formation of pure complex **3** (see Supporting Information). Complex **3** shows an EPR spectrum with an axial signal at $g_{eff} = 3.91$ and 2.00, characteristic of a non-heme hs-{FeNO}^{7} complex with $S_t = 3/2$ (Figure S14). The solid state IR spectrum of **3** shows a typical υ(N-O) = 1742 cm^{-1}. Crystals suitable for X-ray diffraction were obtained via diffusion of pentane into a tetrahydrofuran solution of **3**. The structure of **3** shown in Figure 5 exhibits

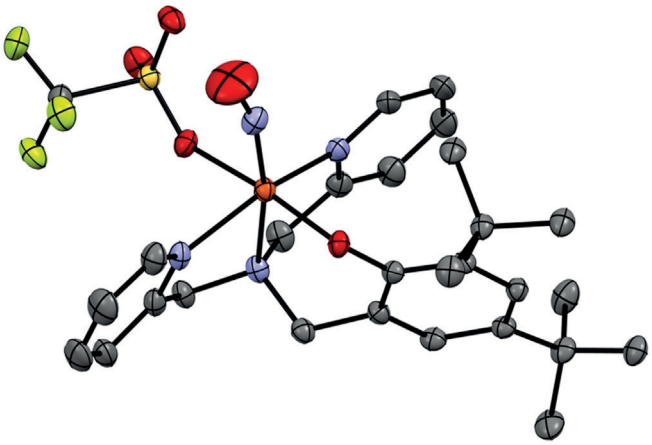

Figure 5. Crystal structure of complex **3** with thermal ellipsoids set at 50% probability. Solvent molecules, and hydrogen atoms are omitted for clarity.[21]

Fe–NO and N–O bond lengths of 1.78 and 1.10 Å, respectively, and an Fe-N-O angle of 163°. The cyclic voltammogram of **3** shows an irreversible signal at −1.07 V versus Fc$^+$/Fc (Figure S12), thus allowing us to use CoCp$_2$ to reduce **3** to the hs-{FeNO}^{8} product, **3red**. Upon reduction with 1 equivalent of CoCp$_2$, the N-O stretch at 1752 cm^{-1} of **3** immediately disappears, and two new features appear at 1632 and 1692 cm^{-1}, which are typical for {Fe(NO)$_2$}^{10} DNICs (Figure S8).[14] However, just as in the previous studies, no intermediate of the process [following Eq. (1)] can be observed.

In conclusion, we have discovered a new structural motif in non-heme iron-nitrosyl chemistry, an Fe$_2$(NO)$_2$ diamond core with two bridging NO ligands (complex **2**), generated from the reduction of the non-heme hs-{FeNO}^{7} complex **1**. We propose that the initially formed {FeNO}^{8} complex (after reduction) is hs, but that upon dimerization the Fe centers undergo a spin crossover to ls, which leads to the stabilization of the Fe$_2$(NO)$_2$ diamond core. The studies on the analogous complex **3** show that this reactivity is unique for the TPA ligand scaffold, which has a ligand field that is on the borderline of spin-crossover. Spectroscopic data show that the dimeric complex **2** contains ls-Fe^{II} with bound ^{1}NO$^-$ ligands, and hence, is diamagnetic. It is of note that dimerization of mononuclear hs-{FeNO}^{8} complexes has been proposed to be the key process in the formation of N$_2$O and DNICs, as also suggested by stoichiometry. To further support the idea that the one-electron reduced form of complex **1** (**1red**) is a hs-{FeNO}^{8} species, DFT calculations were performed on **1red** (with triflate as the 6th ligand) in both the ls and hs state (using B3LYP*/TZVP). The results show that the hs state is clearly the ground state of **1red**, being 15 kcal mol^{-1} lower in energy compared to the ls state. Although previous studies have shown that DNICs are a common reaction product of hs-{FeNO}^{8} complexes, their mechanism of formation has remained elusive. We speculate that the dimeric structure of **2** could be a model for the corresponding intermediate that is responsible for DNIC formation. The {FeNO}^{8} units would remain hs in the dimer, which, after loss of Fe^{II}, generates a DNIC. In this sense, the Fe$_2$(NO)$_2$ structural motif observed in **2** is a perfect template for the formation of DNICs. Further work will now focus on the exact electronic structure and vibrational properties of the highly unusual Fe$_2$(NO)$_2$ core of **2**. Because the N–O stretch of **2** is in an unexpected region, it is possible that these types of intermediates have been overlooked in previous protein and model complex studies. Given the close proximity of the iron centers in iron–sulfur proteins, this type of intermediate could potentially be formed. Nevertheless, whether a bridging structure like **2** exists in nature remains to be seen.

Acknowledgements

This work was supported by the National Science Foundation (CHE-1608331 to N.L.), and the National Institutes of Health (GM-127079 to C.E.K.). A.L.S. acknowledges funding from an NSF-GRFP fellowship and a Rackham predoctoral fellowship. We acknowledge Dr. Jeff Kampf (University of Michigan), funding from NSF grant CHE-0840456 for X-ray instrumentation, and funding from the Robert W. Parry Scholarship and the Eastman Research Fellowship for HTD.

Conflict of interest

The authors declare no conflict of interest.

Keywords: dinitrosyl iron complexes (DNICs) · model complexes · nitric oxide · non-heme iron complexes

How to cite: *Angew. Chem. Int. Ed.* **2019**, *58*, 17695–17699
Angew. Chem. **2019**, *131*, 17859–17863

[1] a) L. Ignarro, *Nitric Oxide: Biology and Pathobiology*, Academic Press, San Diego, **2000**; b) D. A. Wink, J. B. Mitchell, *Free Radical Biol. Med.* **1998**, *25*, 434–456; c) N. Lehnert, H. T. Dong,

J. B. Harland, A. P. Hunt, C. J. White, *Nat. Rev. Chem.* **2018**, *2*, 278.
[2] D. J. Stuehr, S. S. Gross, I. Sakuma, R. Levi, C. F. Nathan, *J. Exp. Med.* **1989**, *169*, 1011.
[3] K. M. Miranda, *Coord. Chem. Rev.* **2005**, *249*, 433 – 455.
[4] R. Lin, P. J. Farmer, *J. Am. Chem. Soc.* **2000**, *122*, 2393 – 2394.
[5] a) A. B. McQuarters, N. E. Wirgau, N. Lehnert, *Curr. Opin. Chem. Biol.* **2014**, *19*, 82 – 89; b) D. Bykov, F. Neese, *Inorg. Chem.* **2015**, *54*, 9303 – 9316.
[6] a) H. T. Dong, C. J. White, B. Zhang, C. Krebs, N. Lehnert, *J. Am. Chem. Soc.* **2018**, *140*, 13429 – 13440; b) C. J. White, A. L. Speelman, C. Kupper, S. Demeshko, F. Meyer, J. P. Shanahan, E. E. Alp, M. Hu, J. Zhao, N. Lehnert, *J. Am. Chem. Soc.* **2018**, *140*, 2562 – 2574.
[7] a) S. Khatua, A. Majumdar, *J. Inorg. Biochem.* **2015**, *142*, 145 – 153; b) D. M. Kurtz, Jr., *Dalton Trans.* **2007**, 4115 – 4121.
[8] A. M. Confer, A. C. McQuilken, H. Matsumura, P. Moënne-Loccoz, D. P. Goldberg, *J. Am. Chem. Soc.* **2017**, *139*, 10621 – 10624.
[9] a) N. Kindermann, A. Schober, S. Demeshko, N. Lehnert, F. Meyer, *Inorg. Chem.* **2016**, *55*, 11538 – 11550; b) Z. J. Tonzetich, F. Héroguel, L. H. Do, S. J. Lippard, *Inorg. Chem.* **2011**, *50*, 1570 – 1579.
[10] a) J. R. Hickok, S. Sahni, H. Shen, A. Arvind, C. Antoniou, L. W. M. Fung, D. D. Thomas, *Free Radical Biol. Med.* **2011**, *51*, 1558 – 1566; b) H. Lewandowska, M. Kalinowska, K. Brzóska, K. Wójciuk, G. Wójciuk, M. Kruszewski, *Dalton Trans.* **2011**, *40*, 8273 – 8289.
[11] B. D'Autréaux, O. Horner, J.-L. Oddou, C. Jeandey, S. Gambarelli, C. Berthomieu, J.-M. Latour, I. Michaud-Soret, *J. Am. Chem. Soc.* **2004**, *126*, 6005 – 6016.
[12] M. Boese, P. I. Mordvintcev, A. F. Vanin, R. Busse, A. Mülsch, *J. Biol. Chem.* **1995**, *270*, 29244 – 29249.
[13] M. Lee, P. Arosio, A. Cozzi, N. D. Chasteen, *Biochemistry* **1994**, *33*, 3679 – 3687.
[14] A. L. Speelman, C. J. White, B. Zhang, E. E. Alp, J. Zhao, M. Hu, C. Krebs, J. Penner-Hahn, N. Lehnert, *J. Am. Chem. Soc.* **2018**, *140*, 11341 – 11359.
[15] J. Wang, C. Li, Q. Zhou, W. Wang, Y. Hou, B. Zhang, X. Wang, *Dalton Trans.* **2016**, *45*, 5439 – 5443.
[16] Y. Zang, J. Kim, Y. Dong, E. C. Wilkinson, E. H. Appelman, L. Que Jr., *J. Am. Chem. Soc.* **1997**, *119*, 4197 – 4205.
[17] V. K. K. Praneeth, C. Näther, G. Peters, N. Lehnert, *Inorg. Chem.* **2006**, *45*, 2795 – 2811.
[18] J. Li, A. Banerjee, P. L. Pawlak, W. W. Brennessel, F. A. Chavez, *Inorg. Chem.* **2014**, *53*, 5414 – 5416.
[19] T. C. Berto, M. B. Hoffman, Y. Murata, K. B. Landenberger, E. E. Alp, J. Zhao, N. Lehnert, *J. Am. Chem. Soc.* **2011**, *133*, 16714 – 16717.
[20] a) K. Fujisawa, S. Soma, H. Kurihara, H. T. Dong, M. Bilodeau, N. Lehnert, *Dalton Trans.* **2017**, *46*, 13273 – 13289; b) C. Van Stappen, N. Lehnert, *Inorg. Chem.* **2018**, *57*, 4252 – 4269.
[21] CCDC 1875658, 1875657, and 1895319 contain the supplementary crystallographic data for this paper. These data can be obtained free of charge from The Cambridge Crystallographic Data Centre.

Manuscript received: September 18, 2019
Accepted manuscript online: September 24, 2019
Version of record online: October 23, 2019

